The Astrophysical Journal, 843:65 (13pp), 2017 July 1 https://doi.org/10.3847/1538-4357/aa7898

Constraints to Dark Energy Using PADE Parameterizations

M. Rezaei[1], M. Malekjani[1], S. Basilakos[2], A. Mehrabi[1], and D. F. Mota[3]
[1] Department of Physics, Bu-Ali Sina University, Hamedan 65178, Iran
[2] Academy of Athens, Research Center for Astronomy and Applied Mathematics, Soranou Efessiou 4, 11-527 Athens, Greece
[3] Institute of Theoretical Astrophysics, University of Oslo, NO 0315 Oslo, Norway
Received 2017 May 4; revised 2017 June 6; accepted 2017 June 7; published 2017 July 5

Abstract

We put constraints on dark energy (DE) properties using PADE parameterization, and compare it to the same constraints using Chevalier–Polarski–Linder (CPL) and ΛCDM, at both the background and the perturbation levels. The DE equation of the state parameter of the models is derived following the mathematical treatment of PADE expansion. Unlike CPL parameterization, PADE approximation provides different forms of the equation of state parameter that avoid the divergence in the far future. Initially we perform a likelihood analysis in order to put constraints on the model parameters using solely background expansion data, and we find that all parameterizations are consistent with each other. Then, combining the expansion and the growth rate data, we test the viability of PADE parameterizations and compare them with CPL and ΛCDM models, respectively. Specifically, we find that the growth rate of the current PADE parameterizations is lower than ΛCDM model at low redshifts, while the differences among the models are negligible at high redshifts. In this context, we provide for the first time a growth index of linear matter perturbations in PADE cosmologies. Considering that DE is homogeneous, we recover the well-known asymptotic value of the growth index (namely $\gamma_\infty = \frac{3(w_\infty - 1)}{6w_\infty - 5}$), while in the case of clustered DE, we obtain $\gamma_\infty \simeq \frac{3w_\infty(3w_\infty - 5)}{(6w_\infty - 5)(3w_\infty - 1)}$. Finally, we generalize the growth index analysis in the case where γ is allowed to vary with redshift, and we find that the form of $\gamma(z)$ in PADE parameterization extends that of the CPL and ΛCDM cosmologies, respectively.

Key words: cosmological parameters – cosmology: theory – dark energy – large-scale structure of universe

1. Introduction

Various independent cosmic observations including those of type Ia supernova (SN Ia; Riess et al. 1998; Perlmutter et al. 1999; Kowalski et al. 2008), cosmic microwave background (CMB; Komatsu et al. 2009; Jarosik et al. 2011; Komatsu et al. 2011; Planck Collaboration XIV 2016), large-scale structure (LSS), baryonic acoustic oscillation (BAO; Tegmark et al. 2004; Cole et al. 2005; Eisenstein et al. 2005; Percival et al. 2010; Blake et al. 2011b; Reid et al. 2012), high redshift galaxies (Alcaniz 2004), high redshift galaxy clusters (Wang & Steinhardt 1998a; Allen et al. 2004), and weak gravitational lensing (Benjamin et al. 2007; Amendola et al. 2008; Fu et al. 2008) reveal that the present universe experiences an accelerated expansion. Within the framework of general relativity (GR), the physical origin of the cosmic acceleration can be described by invoking the existence of an exotic fluid with sufficiently negative pressure, the so-called dark energy (DE). One possibility is that DE consists of the vacuum energy or cosmological constant Λ with constant EoS parameter $w_\Lambda = -1$ (Peebles & Ratra 2003). Alternatively, the fine-tuning and cosmic coincidence problems (Weinberg 1989; Sahni & Starobinsky 2000; Carroll 2001; Padmanabhan 2003; Copeland et al. 2006) led the scientific community to suggest a time-evolving energy density with negative pressure. In those models, the EoS parameter is a function of redshift, $w(z)$ (Caldwell et al. 1998; Armendariz-Picon et al. 2001; Caldwell 2002; Erickson et al. 2002; Padmanabhan 2002; Elizalde et al. 2004). A precise measurement of EoS parameter and its variation with cosmic time can provide important clues about the dynamical behavior of DE and its nature (Copeland et al. 2006; Frieman et al. 2008; Amendola et al. 2013; Weinberg et al. 2013).

One possible way to study the EoS parameter of dynamical DE models is via a parameterization. In literature, one can find many different EoS parameterizations. One of the simplest and earliest parameterizations is the Taylor expansion of $w_{de}(z)$ with respect to redshift z up to first order as $w_{de}(z) = w_0 + w_1 z$ (Maor et al. 2001; Riess et al. 2004). It can also be generalized by considering the second-order approximation in the Taylor series as $w_{de}(z) = w_0 + w_1 z + w_2 z^2$ (Bassett et al. 2008). However, these two parameterizations diverge at high redshifts. Hence the well-known Chevallier–Polarski–Linder (CPL) parameterization, $w_{de}(z) = w_0 + w_1(1 - a) = w_0 + w_1 z/(1 + z)$, was proposed (Chevallier & Polarski 2001; Linder 2003). The CPL parameterization can be considered as a Taylor series with respect to $(1 - a)$ and was extended to a more general case by assuming the second-order approximation as $w_{de}(a) = w_0 + w_1(1 - a) + w_2(1 - a)^2$ (Seljak et al. 2005). In addition to the CPL formula, some purely phenomenological parameterizations have been proposed more recently. For example, $w_{de}(z) = w_0 + w_1 z/(1 + z)^\alpha$, where α is fixed to 2 (Jassal et al. 2005). In this class, the power law $w_{de}(a) = w_0 + w_1(1 - a^\beta)/\beta$ (Barboza et al. 2009) and logarithmic $w_{de}(a) = w_0 + w_1 \ln a$ (Efstathiou 1999) parameterizations have been investigated. Another logarithm parameterization is $w_{de}(z) = w_0/[1 + b\ln(1 + z)]^\alpha$, where α is taken to be 1 or 2 (Wetterich 2004). Notice that although the CPL is a well-behaved parameterization at early ($a \ll 1$) and present ($a \sim 1$) epochs, it diverges when the scale factor goes to infinity. This is also a common difficulty for the previously noted phenomenological parameterizations. Recently, to solve the divergence, several phenomenological parameterizations have been introduced (see Dent et al. 2009; Frampton & Ludwick 2011; Feng et al. 2012, for more details). Notice that most of these EoS parameterizations are ad hoc and purely written by hand, where there is no mathematical principle or

fundamental physics behind them. In this work we focus on PADE parameterization (see Section 2), which from the mathematical point of view seems to be more stable: it does not diverge and can be employed at both small and high redshifts. Using the different types of PADE parameterizations to express the EoS parameter of DE w_{de} in terms of redshift z, we study the growth of perturbations in the universe.

DE not only accelerates the expansion rate of the universe but also changes the evolution of growth rate of matter perturbations and consequently the formation epochs of LSSs of universe (Armendariz-Picon et al. 1999; Garriga & Mukhanov 1999; Armendariz-Picon et al. 2000; Tegmark et al. 2004; Pace et al. 2010; Akhoury et al. 2011). Moreover, the growth of cosmic structures are also affected by perturbations of DE when we deal with dynamical DE models with time varying EoS parameter $w_{de} \neq -1$ (Erickson et al. 2002; Bean & Doré 2004; Hu & Scranton 2004; Basilakos & Voglis 2007; Koivisto & Mota 2007; Mota et al. 2007; Ballesteros & Riotto 2008; Basilakos et al. 2009a, 2010; Gannouji et al. 2010; Sapone & Majerotto 2012; Batista & Pace 2013; Dossett & Ishak 2013; Basse et al. 2014; Batista 2014; Nesseris & Sapone 2015; Pace et al. 2014a, 2014b; Basilakos 2015; Mehrabi et al. 2015a, 2015b, 2015c; Malekjani et al. 2015, 2017).

In addition to the background geometrical data, the data coming from the formation of LSSs provide a valuable information about the nature of DE. In particular, we can set up a more general formalism in which the background expansion data, including SN Ia, BAO, CMB shift parameter, Hubble expansion data, joined with the growth rate data of LSSs in order to put constraints on the parameters of cosmology and DE models (see Cooray et al. 2004; Corasaniti et al. 2005; Koivisto & Mota 2007; Mota et al. 2007, 2008; Basilakos et al. 2010; Gannouji et al. 2010; Mota et al. 2010; Blake et al. 2011b; Nesseris et al. 2011; Basilakos & Pouri 2012; Chuang et al. 2013; Contreras et al. 2013; Llinares & Mota 2013; Llinares et al. 2014; Li et al. 2014; Yang et al. 2014; Basilakos 2015; Mehrabi et al. 2015a, 2015b; Basilakos 2016; Bonilla Rivera & Farieta 2016; Fay 2016; Malekjani et al. 2017).

In this work, following the lines of the previous studies and using the latest observational data, including the geometrical data set (SN Ia, BAO, CMB, big bang nucleosynthesis [BBN], $H(z)$) combined with growth rate data $f(z)\sigma_8$, we perform an overall likelihood statistical analysis to place constraints and find best-fit values of the cosmological parameters where the EoS parameter of DE is approximated by PADE parameterizations. Previously, PADE parameterizations have been studied from different observational tests in cosmology. For example, in Gruber & Luongo (2014), the cosmography analysis has been investigated using PADE approximation. In Wei et al. (2014), the authors proposed several parameterizations for EoS of DE on the basis of PADE approximation. Confronting these EoS parameterizations with the latest geometrical data, they found that PADE parameterizations can work well (for similar studies, see Aviles et al. 2014; Zaninetti 2016; Zhou et al. 2016). Here, for the first time, we study the growth of perturbations in PADE cosmologies. After introducing the main ingredients of PADE parameterizations in Section 2, we study the background evolution of the universe in Section 3. We implement the likelihood analysis using the geometrical data to put constraints on the cosmological and model parameters in PADE parameterizations. In Section 4, the growth of perturbations in PADE cosmologies is investigated. Then we perform an overall likelihood analysis, including the geometrical + growth rate data, to place constraints and obtain the best-fit values of the corresponding cosmological parameters. Finally, we provide the main conclusions in Section 5.

2. PADE Parameterizations

For an arbitrary function $f(x)$, PADE approximate of order (m, n) is given by the following rational function (Pade 1892; Baker & Graves-Morris 1996; Adachi & Kasai 2012)

$$f(x) = \frac{a_0 + a_1 x + a_2 x^2 + ... + a_n x^n}{b_0 + b_1 x + b_2 x^2 + ... + b_n x^m}, \quad (1)$$

where exponents (m, n) are positive and the coefficients (a_i, b_i) are constants. Obviously, for $b_i = 0$ (with $i \geqslant 1$), the current approximation reduces to standard Taylor expansion. In this study we focus on three PADE parameterizations introduced as follows (see also Wei et al. 2014).

2.1. PADE (I)

Based on Equation (1), we first expand the EoS parameter w_{de} with respect to $(1 - a)$ up to order (1, 1) as follows (see also Wei et al. 2014):

$$w_{de}(a) = \frac{w_0 + w_1(1 - a)}{1 + w_2(1 - a)}. \quad (2)$$

From this point forward, we will refer to the previous formula as PADE (I) parameterization. In terms of redshift z, Equation (2) is written as

$$w_{de}(z) = \frac{w_0 + (w_0 + w_1)z}{1 + (1 + w_2)z}. \quad (3)$$

As expected for $w_2 = 0$, Equation (2) boils down to CPL parameterization. Unlike CPL parameterization, here the EoS parameter with $w_2 \neq 0$ avoids the divergence at $a \to \infty$ (or equivalently at $z = -1$). Using Equation (2), we find the following special cases regarding the EoS parameter (see also Wei et al. 2014):

$$w_{de} = \begin{cases} \frac{w_0 + w_1}{1 + w_2}, & \text{for } a \to 0\ (z \to \infty,\ \text{early time}), \\ w_0, & \text{for } a = 1\ (z = 0,\ \text{present}), \\ \frac{w_1}{w_2}, & \text{for } a \to \infty\ (z \to -1,\ \text{far future}), \end{cases} \quad (4)$$

where we need to set $w_2 \neq 0$ and -1. Therefore we argue that the PADE (I) formula is a well-behaved function in the range of $0 \leqslant a \leqslant \infty$ (or equivalently at $-1 \leqslant z \leqslant \infty$).

2.2. Simplified PADE (I)

Clearly PADE (I) approximation has three free parameters: w_0, w_1, and w_2. Setting $w_1 = 0$, we provide a simplified version of PADE (I) parameterization—namely,

$$w_{de}(a) = \frac{w_0}{1 + w_2(1 - a)}. \quad (5)$$

Notice that in order to avoid singularities in the cosmic expansion, w_2 needs to lie in the interval $-1 < w_2 < 0$.

2.3. PADE (II)

Unlike the previous cases, here the current parameterization is written as a function of $N = \ln a$. In this context, the EoS parameter up to order (1, 1) takes the form

$$w_{\rm de}(a) = \frac{w_0 + w_1 \ln a}{1 + w_2 \ln a}, \tag{6}$$

where w_0, w_1, and w_2 are constants (see also Wei et al. 2014). In PADE (II) parameterization, we can easily show that

$$w_{\rm de} = \begin{cases} \frac{w_1}{w_2}, & \text{for } a \to 0\ (z \to \infty,\ \text{early time}), \\ w_0, & \text{for } a = 1\ (z = 0,\ \text{present}), \\ \frac{w_1}{w_2}, & \text{for } a \to \infty\ (z \to -1,\ \text{far future}). \end{cases} \tag{7}$$

Notice that in order to avoid singularities at these epochs, we need to impose $w_2 \neq 0$.

3. Background History in PADE Parameterizations

In this section based on the aforementioned parameterizations, we study the background evolution in PADE cosmologies. Generally speaking, for isotropic and homogeneous spatially flat FRW cosmologies, driven by radiation, nonrelativistic matter, and an exotic fluid with an equation of state $p_{\rm de} = w_{\rm de}\rho_{\rm de}$, the first Friedmann equation reads

$$H^2 = \frac{8\pi G}{3}(\rho_{\rm r} + \rho_{\rm m} + \rho_{\rm de}), \tag{8}$$

where $H \equiv \dot{a}/a$ is the Hubble parameter, and $\rho_{\rm r}$, $\rho_{\rm m}$, and $\rho_{\rm de}$ are the energy densities of radiation, dark matter, and DE, respectively. In the absence of interactions among the three fluids, the corresponding energy densities satisfy the following differential equations:

$$\dot{\rho_{\rm r}} + 4H\rho_{\rm r} = 0, \tag{9}$$

$$\dot{\rho_{\rm m}} + 3H\rho_{\rm m} = 0, \tag{10}$$

$$\dot{\rho_{\rm de}} + 3H(1 + w_{\rm de})\rho_{\rm de} = 0, \tag{11}$$

where the over-dot denotes a derivative with respect to cosmic time t. Based on Equations (9) and (10), it is easy to derive the evolution of radiation and pressureless matter—namely, $\rho_{\rm r} = \rho_{\rm r0}a^{-4}$ and $\rho_{\rm m} = \rho_{\rm m0}a^{-3}$. Inserting Equations (2), (5), and (6) into Equation (11), we can obtain the DE density of the current PADE parameterizations (see also Wei et al. 2014):

$$\rho_{\rm de}^{\rm (PADEI)} = \rho_{\rm de}^{(0)} a^{-3\left(\frac{1+w_0+w_1+w_2}{1+w_2}\right)} [1 + w_2(1-a)]^{-3\left(\frac{w_1-w_0w_2}{w_2(1+w_2)}\right)}, \tag{12}$$

$$\rho_{\rm de}^{\rm (simp.PADEI)} = \rho_{\rm de}^{(0)} a^{-3\left(\frac{1+w_0+w_2}{1+w_2}\right)} [1 + w_2(1-a)]^{-3\left(\frac{-w_0w_2}{w_2(1+w_2)}\right)}, \tag{13}$$

$$\rho_{\rm de}^{\rm (padeII)} = \rho_{\rm de}^{0} a^{-3\left(\frac{w_1+w_2}{w_2}\right)} (1 + w_2 \ln a)^{3\left(\frac{w_1-w_0w_2}{w_2^2}\right)}. \tag{14}$$

Also, combining Equations (12)–(14) and Equation (8), we derive the dimensionless Hubble parameter $E = H/H_0$ (see also Wei et al. 2014). Specifically, we find

$$E^2_{\rm PADE\ I} = \Omega_{\rm r0}a^{-4} + \Omega_{\rm m0}a^{-3} + (1 - [\Omega_{\rm r0} + \Omega_{\rm m0}]) \times a^{-3\left(\frac{1+w_0+w_1+w_2}{1+w_2}\right)} \times (1 + w_2 - aw_2)^{-3\left(\frac{w_1-w_0w_2}{w_2(1+w_2)}\right)}, \tag{15}$$

$$E^2_{\rm simPADE\ I} = \Omega_{\rm r0}a^{-4} + \Omega_{\rm m0}a^{-3} + (1 - [\Omega_{\rm r0} + \Omega_{\rm m0}]) \times a^{-3\left(\frac{1+w_0+w_2}{1+w_2}\right)} \times (1 + w_2 - aw_2)^{-3\left(\frac{-w_0w_2}{w_2(1+w_2)}\right)}, \tag{16}$$

$$E^2_{\rm PADE\ II} = \Omega_{\rm r0}a^{-4} + \Omega_{\rm m0}a^{-3} + (1 - [\Omega_{\rm r0} + \Omega_{\rm m0}]) \times a^{-3\left(\frac{w_1+w_2}{w_2}\right)} \times (1 + w_2 \ln a)^{3\left(\frac{w_1-w_0w_2}{w_2^2}\right)}, \tag{17}$$

where $\Omega_{\rm m0}$ (density parameter), $\Omega_{\rm r0}$ (radiation parameter), and $\Omega_{\rm de0} = 1 - \Omega_{\rm m0} - \Omega_{\rm r0}$ (DE parameter). Moreover, following the previously listed lines in the case of CPL parameterization, we have

$$\rho_{\rm de}^{\rm CPL} = \rho_{\rm de}^{(0)} a^{-3(1+w_0+w_1)} \exp\{-3w_1(1-a)\} \tag{18}$$

and

$$E^2_{\rm CPL} = \Omega_{\rm r0}a^{-4} + \Omega_{\rm m0}a^{-3} + (1 - \Omega_{\rm m0} - \Omega_{\rm r0}) \times a^{-3(1+w_0+w_1)} \exp[-3w_1(1-a)]. \tag{19}$$

We now turn to study the performance of PADE cosmological parameterization against the latest observational data. Specifically, we implement a statistical analysis using the background expansion data including those of SN Ia (Suzuki et al. 2012), BAO (Beutler et al. 2011; Blake et al. 2011a; Padmanabhan et al. 2012; Anderson et al. 2013), CMB (Hinshaw et al. 2013), BBN (Burles et al. 2001; Serra et al. 2009), and Hubble data (Gaztanaga et al. 2009; Blake et al. 2012; Moresco et al. 2012; Anderson et al. 2014). For more details concerning the expansion data, the $\chi^2(p)$ function, the Markov chain Monte Carlo (MCMC) analysis, the Akaike information criterion (AIC), and the Bayesian information criterion (BIC), we refer the reader to Mehrabi et al. (2015b; see also Basilakos et al. 2009b; Hinshaw et al. 2013; Mehrabi et al. 2015a, 2017; Malekjani et al. 2017). In this framework, the joint likelihood function is the product of the individual likelihoods,

$$\mathcal{L}_{\rm tot}(\boldsymbol{P}) = \mathcal{L}_{\rm sn} \times \mathcal{L}_{\rm bao} \times \mathcal{L}_{\rm cmb} \times \mathcal{L}_{\rm h} \times \mathcal{L}_{\rm bbn}, \tag{20}$$

which implies that the total chi-square $\chi^2_{\rm tot}$ is given by

$$\chi^2_{\rm tot}(\boldsymbol{P}) = \chi^2_{\rm sn} + \chi^2_{\rm bao} + \chi^2_{\rm cmb} + \chi^2_{\rm h} + \chi^2_{\rm bbn}, \tag{21}$$

where the statistical vector $\boldsymbol{P}$ includes the free parameters of the model. In our work, the previous vector becomes (a) $\boldsymbol{P} = \{\Omega_{\rm DM0}, \Omega_{\rm b0}, h, w_0, w_1, w_2\}$ for PADE (I) and (II) parameterizations, (b) $\boldsymbol{P} = \{\Omega_{\rm DM0}, \Omega_{\rm b0}, h, w_0, w_2\}$ for simplified PADE (I), and (c) $\boldsymbol{P} = \{\Omega_{\rm DM0}, \Omega_{\rm b0}, h, w_0, w_1\}$ in the case of CPL parameterization. Notice that we utilize $\Omega_{\rm m0} = \Omega_{\rm DM0} + \Omega_{\rm b0}$ and $h = H_0/100$, while the energy density of radiation is fixed to $\Omega_{\rm r0} = 2.469 \times 10^{-5}h^{-2}(1.6903)$ (Hinshaw et al. 2013).

In addition, we utilize the well-known information criteria, namely AIC (Akaike 1974) and BIC (Schwarz 1978), in order to test the statistical performance of the cosmological models themselves. In particular, AIC and BIC are given by

$$\begin{aligned} \text{AIC} &= -2\ln\mathcal{L}_{\rm max} + 2k, \\ \text{BIC} &= -2\ln\mathcal{L}_{\rm max} + k\ln N, \end{aligned} \tag{22}$$

where k is the number of free parameters and N is the total number of observational data points. The results of our statistical analysis are presented in Tables 1 and 2, respectively. Although the current DE parameterizations provide low AIC

Table 1
Statistical Results for the Various DE Parameterizations Used in the Analysis

Model	PADE I	Simp. PADE I	PADE II	CPL	ΛCDM
k	6	5	6	5	3
$\chi^2_{\rm min}$	567.6	567.7	567.9	567.6	574.4
AIC	579.6	577.7	579.9	577.6	580.4
BIC	606.1	599.8	606.4	599.7	593.6

Note. These results are based on the expansion data. The concordance ΛCDM model is shown for comparison.

values with respect to those of ΛCDM, we find $\Delta{\rm AIC} = {\rm AIC} - {\rm AIC}_\Lambda < 4$; hence the DE parameterizations explored in this study are consistent with the expansion data. In order to visualize the solution space of the model parameters in Figure 1, we present the 1σ, 2σ, and 3σ confidence levels for various parameter pairs. Using the best-fit model parameters (see Table 2) in Figure 2, we plot the redshift evolution of $w_{\rm de}$ (upper panel), $\Delta E(\%) = [(E - E_\Lambda)/E_\Lambda] \times 100$ (middle panel), and $\Omega_{\rm de}$ (lower panel). The different parameterizations are characterized by the colors and line types presented in the caption of Figure 2. We find that the EoS parameter of PADE II evolves only in the quintessence regime ($-1 < w_{\rm de} < -1/3$). For the other DE parameterizations, we observe that $w_{\rm de}$ varies in the phantom region ($w_{\rm de} < -1$) at high redshifts, while it enters in the quintessence regime ($-1 < w_{\rm de} < -1/3$) at relatively low redshifts. Notice that the present value of $w_{\rm de}$ can be found in Table 2. From the middle panel of Figure 2, we observe that the relative difference ΔE is close to 2%–3.5% at low redshifts ($z \sim 0.5$), while in the case of PADE (II), we always have $E_{\rm PADE\ II}(z) > E_\Lambda(z)$. Lastly, in the bottom panel of Figure 2, we show the evolution of $\Omega_{\rm de}$, where its current value can be found in Table 2. As expected, $\Omega_{\rm de}$ tends to zero at high redshifts, since matter dominates the cosmic fluid. In the case of PADE parameterizations, we observe that $\Omega_{\rm de}$ is larger than that of the usual Λ cosmology.

Finally, we would like to estimate the transition redshift $z_{\rm tr}$ of the PADE parameterizations by utilizing the deceleration parameter $q(z) = -1 - \dot{H}/H^2$. Following standard lines, it is easy to show

$$\frac{\dot{H}}{H^2} = -\frac{3}{2}(1 + w_{\rm de}(z)\Omega_{\rm de}(z)). \tag{23}$$

which implies that

$$q(z) = \frac{1}{2} + \frac{3}{2}w_{\rm de}(z)\Omega_{\rm de}(z). \tag{24}$$

Using the best-fit values of Table 2, we plot in Figure 3 the evolution of q for the current DE parameterizations. In all cases, including that of ΛCDM, q tends to $1/2$ at early enough times. This is expected, since the universe is matter dominated ($\Omega_{\rm de} \simeq 0$) at high redshifts. Now solving the $q(z_{\rm tr}) = 0$, we can derive the transition redshift—namely, the epoch at which the expansion of the universe starts to accelerate. In particular, we find $z_{\rm tr} = 0.86$ (PADE I), $z_{\rm tr} = 0.84$ (simplified PADE), $z_{\rm tr} = 0.72$ (PADE II), $z_{\rm tr} = 0.80$ (CPL), and $z_{\rm tr} = 0.71$ (ΛCDM). The latter results are in good agreement with the measured $z_{\rm tr}$ based on the cosmic chronometer $H(z)$ data Farooq et al. (2017; see also Capozziello et al. 2014, 2015).

4. Growth Rate in DE Parameterizations

In this section, we study the linear growth of matter perturbations in PADE cosmologies, and we compare them with those of CPL and ΛCDM, respectively. In this kind of study, the natural question to ask is the following: How does DE affect the linear growth of matter fluctuations? In order to answer this question, we need to introduce the following two distinct situations, which have been considered within different approaches in the literature (Armendariz-Picon et al. 1999; Garriga & Mukhanov 1999; Armendariz-Picon et al. 2000; Erickson et al. 2002; Bean & Doré 2004; Hu & Scranton 2004; Abramo et al. 2007, 2008; Ballesteros & Riotto 2008; Abramo et al. 2009; Basilakos et al. 2009a; de Putter et al. 2010; Pace et al. 2010; Akhoury et al. 2011; Sapone & Majerotto 2012; Pace et al. 2012; Batista & Pace 2013; Dossett & Ishak 2013; Batista 2014; Basse et al. 2014; Pace et al. 2014a, 2014b; Malekjani et al. 2015; Naderi et al. 2015; Mehrabi et al. 2015a, 2015b, 2015c; Nazari-Pooya et al. 2016; Malekjani et al. 2017): (i) the scenario in which the DE component is homogeneous ($\delta_{\rm de} \equiv 0$) and only the corresponding non-relativistic matter is allowed to cluster ($\delta_{\rm m} \neq 0$) and (ii) the case in which the whole system clusters (both matter and DE). Owing to the fact that we are in the matter phase of the universe, we can neglect the radiation term from the Hubble expansion.

4.1. Basic Equations

The basic equations that govern the evolution of non-relativistic matter and DE perturbations are given by (Abramo et al. 2009)

$$\dot{\delta_{\rm m}} + \frac{\theta_{\rm m}}{a} = 0, \tag{25}$$

$$\dot{\delta_{\rm de}} + (1 + w_{\rm de})\frac{\theta_{\rm de}}{a} + 3H(c^2_{\rm eff} - w_{\rm de})\delta_{\rm de} = 0, \tag{26}$$

$$\dot{\theta_{\rm m}} + H\theta_{\rm m} - \frac{k^2\phi}{a} = 0, \tag{27}$$

$$\dot{\theta_{\rm de}} + H\theta_{\rm de} - \frac{k^2 c^2_{\rm eff}\theta_{\rm de}}{(1 + w_{\rm de})a} - \frac{k^2\phi}{a} = 0, \tag{28}$$

where k is the wave number and $c_{\rm eff}$ is the effective sound speed of perturbations (Abramo et al. 2009; Batista & Pace 2013; Batista 2014). Combining the Poisson equation,

$$-\frac{k^2}{a^2}\phi = \frac{3}{2}H^2[\Omega_{\rm m}\delta_{\rm m} + (1 + 3c^2_{\rm eff})\Omega_{\rm de}\delta_{\rm de}], \tag{29}$$

with Equations (27) and (28), eliminating $\theta_{\rm m}$ and $\theta_{\rm de}$, and changing the derivative from time to scale factor a, we obtain the following system of differential equations (see also Mehrabi

Table 2
Summary of the Best-fit Parameters for the Various DE Parameterizations Using the Background Data

Model	PADE I	Simplified PADE I	PADE II	CPL	ΛCDM
$\Omega_{\rm m}^{(0)}$	0.286 ± 0.010	0.270 ± 0.010	0.2864 ± 0.0096	0.2896 ± 0.0090	0.2891 ± 0.0090
h	0.682 ± 0.012	0.682 ± 0.012	0.686 ± 0.013	0.682 ± 0.012	0.6837 ± 0.0084
w_0	-0.825 ± 0.091	-0.845 ± 0.039	-0.889 ± 0.080	-0.80 ± 0.11	⋯
w_1	$-0.09^{+0.39}_{-0.32}$	⋯	$0.37^{+0.29}_{-0.23}$	$-0.51^{+0.48}_{-0.38}$	⋯
w_2	$-0.683^{+0.040}_{-0.034}$	-0.387 ± 0.034	$-0.353^{+0.038}_{-0.034}$	⋯	⋯
$w_{\rm de}(z=0)$	-0.825	-0.845	-0.889	-0.80	-1.0
$\Omega_{\rm de}(z=0)$	0.714	0.730	0.7136	0.7104	0.7109

et al. 2015a; Malekjani et al. 2017):

$$\delta_{\rm m}'' + \frac{3}{2a}(1 - w_{\rm de}\Omega_{\rm de})\delta_{\rm m}' = \frac{3}{2a^2} \times [\Omega_{\rm m}\delta_{\rm m} + \Omega_{\rm de}(1 + 3c_{\rm eff}^2)\delta_{\rm de}], \quad (30)$$

$$\delta_{\rm de}'' + A\delta_{\rm de}' + B\delta_{\rm de} = \frac{3}{2a^2}(1 + w_{\rm de}) \times [\Omega_{\rm m}\delta_{\rm m} + \Omega_{\rm de}(1 + 3c_{\rm eff}^2)\delta_{\rm de}]. \quad (31)$$

In the following analysis, we set $c_{\rm eff} \equiv 0$, which means that the whole system (matter and DE) fully clusters. Moreover, we remind the reader that for homogeneous DE models we have $\delta_{\rm de} \equiv 0$; hence Equation (30) reduces to the well-known differential equation of Peebles (1993; see also Pace et al. 2010 and references therein). Concerning the functional forms of A and B, we have

$$A = \frac{1}{a}\left[-3w_{\rm de} - \frac{aw_{\rm de}'}{1 + w_{\rm de}} + \frac{3}{2}(1 - w_{\rm de}\Omega_{\rm de})\right],$$
$$B = \frac{1}{a^2}\left[-aw_{\rm de}' + \frac{aw_{\rm de}'w_{\rm de}}{1 + w_{\rm de}} - \frac{1}{2}w_{\rm de}(1 - 3w_{\rm de}\Omega_{\rm de})\right]. \quad (32)$$

In order to perform the numerical integration of the system indicated in (30) and (31), it is crucial to introduce the appropriate initial conditions. Here we utilize (see also Batista & Pace 2013; Mehrabi et al. 2015a; Malekjani et al. 2017)

$$\delta_{\rm mi}' = \frac{\delta_{\rm mi}}{a_{\rm i}},$$
$$\delta_{\rm dei} = \frac{1 + w_{\rm dei}}{1 - 3w_{\rm dei}}\delta_{\rm mi},$$
$$\delta_{\rm dei}' = \frac{4w_{\rm dei}'}{(1 - 3w_{\rm dei})^2}\delta_{\rm mi} + \frac{1 + w_{\rm dei}}{1 - 3w_{\rm dei}}\delta_{\rm mi}', \quad (33)$$

where we fix $a_{\rm i} = 10^{-4}$ and $\delta_{\rm mi} = 1.5 \times 10^{-5}$. In fact, using the aforementioned conditions, we verify that matter perturbations always stay in the linear regime. From the technical viewpoint, using $w_{\rm de}$, $\Omega_{\rm de}$, we can solve the system of Equations (30) and (31), which means that the fluctuations ($\delta_{\rm de}$, $\delta_{\rm m}$) can be readily calculated, and from them $f(z) = d\ln\delta_{\rm m}/d\ln a$, $\sigma_8(z) = \frac{\delta_{\rm m}(z)}{\delta_{\rm m}(z=0)}\sigma_8(z=0)$ (rms mass variance at $R = 8h^{-1}$ Mpc), and $f(z)\sigma_8(z)$ immediately ensue.

Now we perform a joint statistical analysis involving the expansion data (see Section 3) and the growth data. In principle, this can help us to better understand the theoretical expectations of the present DE parameterizations, as well as test their behavior in the background and at the perturbation level. The growth data and the details regarding the likelihood analysis ($\chi^2_{\rm gr}$, MCMC algorithm, etc.) can be found in Section 3 of our previous work (Mehrabi et al. 2015a). Briefly, in order to obtain the overall likelihood function, we need to include the likelihood function of the growth data in Equation (20) as follows:

$$\mathcal{L}_{\rm tot}(\boldsymbol{P}) = \mathcal{L}_{\rm sn} \times \mathcal{L}_{\rm bao} \times \mathcal{L}_{\rm cmb} \times \mathcal{L}_{\rm h} \times \mathcal{L}_{\rm bbn} \times \mathcal{L}_{\rm gr}, \quad (34)$$

and hence

$$\chi^2_{\rm tot}(\boldsymbol{P}) = \chi^2_{\rm sn} + \chi^2_{\rm bao} + \chi^2_{\rm cmb} + \chi^2_{\rm h} + \chi^2_{\rm bbn} + \chi^2_{\rm gr}, \quad (35)$$

where the statistical vector $\boldsymbol{P}$ contains an additional free parameter—namely, $\sigma_8 \equiv \sigma_8(z=0)$.

In Tables 3 and 4 we show the resulting best-fit values for various DE parameterizations under investigation, in which we also provide the observational constraints of the clustered DE parameterizations. Furthermore, in Figure 4 we present the 1σ and 2σ contours for various parameter pairs. The blue contour represents the confidence levels based on geometrical data and green (red) contours show the confidence levels based on geometrical + growth rate data for clustered (homogeneous) DE parameterizations. Comparing the latter results with those of see Section 3, we conclude that the observational constraints that are placed by the expansion + growth data are practically the same as those found by the expansion data. Therefore, we can use the current growth data in order to put constrains only on σ_8, since they do not significantly affect the rest of the cosmological parameters. This means that the results of Section 3 concerning the evolution of the main cosmological functions ($w_{\rm de}$, $E(z)$, and $\Omega_{\rm de}$) remain unaltered. To this end, in Figure 5 we plot the evolution of growth rate $f(z)$ as a function of redshift (upper panel) and the fractional difference with respect to that of the ΛCMD model (lower panel), $\Delta f(\%) = 100 \times [f(z) - f_\Lambda(z)]/f_\Lambda(z)$. Specifically, in the range of $0 \leqslant z \leqslant 4$, we find the following:

1. For homogeneous (or clustered) PADE I parameterization, the relative difference is $\sim[-1\%, 1\%]$ (or $\sim[-2.25\%, 1\%]$).
2. In the case of simplified PADE I, we have $\sim[-1\%, 0.4\%]$ and $\sim[-1\%, 0.4\%]$ for homogeneous and clustered DE, respectively.
3. For homogeneous (or clustered) PADE II DE, the relative deviation lies in the interval $\sim[-4.25\%, -0.25\%]$ (or $\sim[-4\%, -0.25\%]$). Finally, in the case of CPL parameterization, we obtain $\sim[-1.5\%, 0.1\%]$ (homogeneous) and $\sim[-1\%, 0.1\%]$ (clustered).

In this context, we verify that at high redshifts the growth rate tends to unity, since the universe is matter-dominated—namely, $\delta_{\rm m} \propto a$. Moreover, we observe that the evolution of Δf has one

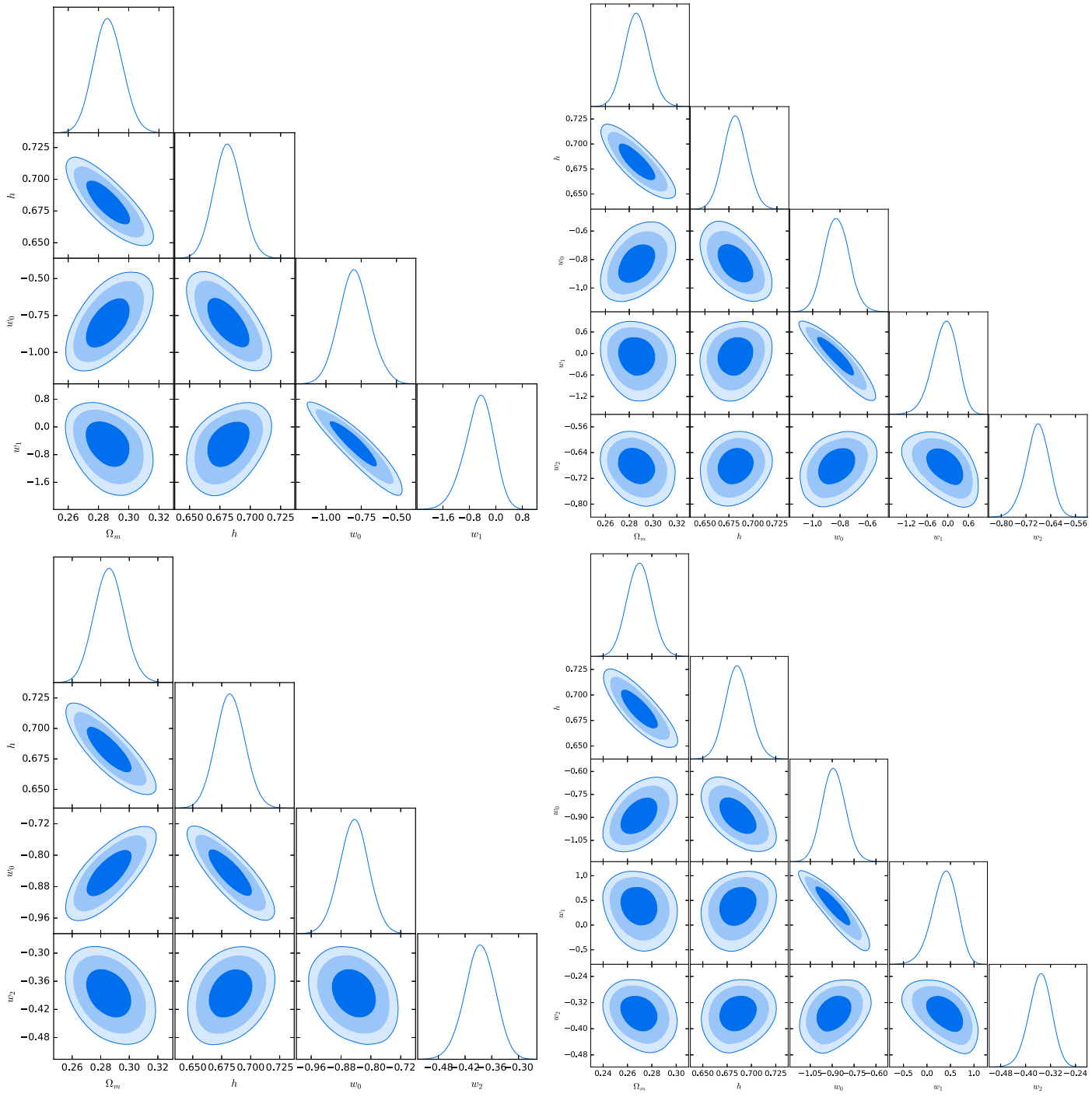

Figure 1. 1σ, 2σ, and 3σ likelihood contours for various cosmological parameters using the latest expansion data. The upper left (upper right) panel shows the results for CPL (PADE I) parameterization. The lower left (lower right) panel shows the results for simplified PADE I (PADE II) parameterization.

maximum/minimum and one zero point. As expected, this feature of Δf is related to the evolution of ΔE (see the middle panel of Figure 2). Indeed, we verify that large values of the normalized Hubble parameter $E(z)$ correspond to small values of the growth rate. Also, looking at Figure 2 (middle panel) and Figure 5 (bottom panel), we easily see that when ΔE has a maximum, the growth rate Δf has a minimum and vice versa. We also observe that if $\Delta E < 0$, then $\Delta f > 0$ and vice versa. Finally, in Figure 6, we compare the observed $f\sigma_8(z)$ with the predicted growth rate function of the current DE parameterizations (for curves, see the caption of Figure 6). We find that all parameterizations represent the growth data well. As expected from AIC and BIC analysis (see Table 3), the current DE parameterizations and standard ΛCDM cosmology are all consistent with current observational data.

4.2. The Growth Index

We would like to finish this section with a discussion concerning the growth index of matter fluctuations γ, which affects the growth rate of clustering via the following relation

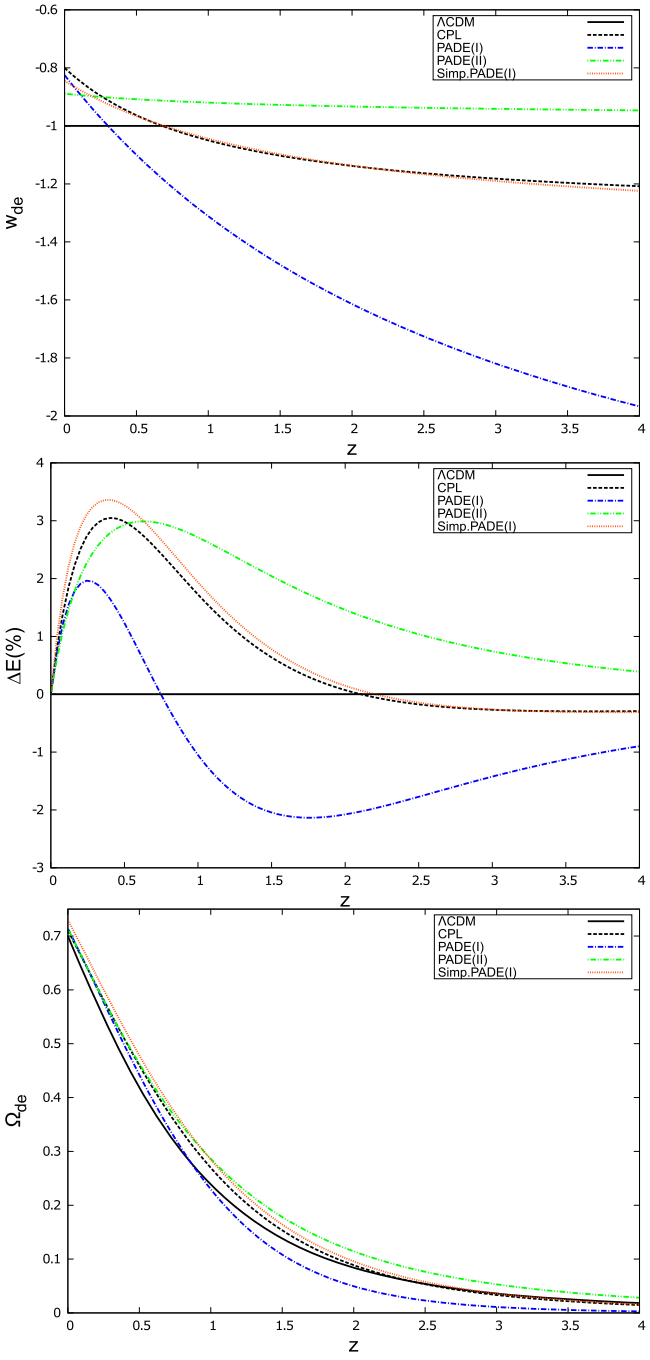

Figure 2. Redshift evolution of various cosmological quantities—namely, dark energy EoS parameter $w_{\rm de}(z)$ (top panel), relative deviation $\Delta E(\%) = [(E - E_\Lambda)/E_\Lambda] \times 100$ (middle panel), and $\Omega_{\rm de}(z)$ (bottom panel). The different DE parameterizations are characterized by the colors and line types presented in the inner panels of the figure.

(first introduced by Peebles 1993):

$$f(z) = \frac{d\ln\delta_{\rm m}}{d\ln a}(z) \simeq \Omega_{\rm m}^{\gamma}(z). \tag{36}$$

The theoretical formula of the growth index has been studied for various cosmological models, including scalar field DE (Silveira & Waga 1994; Wang & Steinhardt 1998b; Linder & Jenkins 2003; Lue et al. 2004; Linder & Cahn 2007; Nesseris & Perivolaropoulos 2008), DGP (Linder & Cahn 2007; Gong 2008; Wei 2008; Fu et al. 2009), Finsler–Randers (Basilakos & Stavrinos 2013), running vacuum $\Lambda(H)$ (Basilakos & Sola 2015), $f(R)$ (Gannouji et al. 2009; Tsujikawa et al. 2009), $f(T)$ (Basilakos 2016), holographic DE (Mehrabi et al. 2015a), and agegraphic DE (Malekjani et al. 2017). If we combine Equations (25)–(29) simultaneously using $\frac{d\delta_{\rm m}}{dt} = aH\frac{d\delta_{\rm m}}{da}$, then we obtain (see also Abramo et al. 2007, 2009; Mehrabi et al. 2015a)

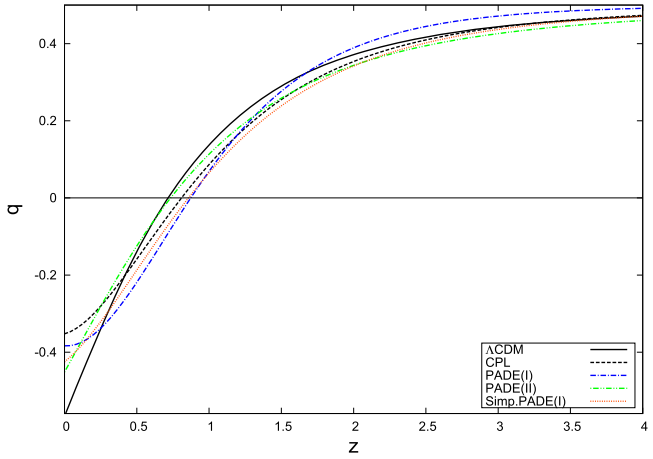

Figure 3. Evolution of the deceleration parameter q for different PADE parameterizations considered in this work. The CPL and ΛCDM models are shown for comparison.

$$a^2\delta_{\rm m}'' + a\left(3 + \frac{\dot{H}}{H^2}\right)\delta_{\rm m}' = \frac{3}{2}\Omega_{\rm m}\mu, \tag{37}$$

where

$$\frac{\dot{H}}{H^2} = \frac{d\ln H}{d\ln a} = -\frac{3}{2} - \frac{3}{2}w_{\rm de}(a)\Omega_{\rm de}(a), \tag{38}$$

and $\Omega_{\rm de}(a) = 1 - \Omega_{\rm m}(a)$. The quantity $\mu(a)$ characterizes the nature of DE in PADE parameterizations—namely,

$$\mu(a) = \begin{cases} 1 & \text{Homogeneous PADE} \\ 1 + \dfrac{\Omega_{\rm de}(a)}{\Omega_{\rm m}(a)}\Delta_{\rm de}(a)(1 + 3c_{\rm eff}^2) & \text{Clustered PADE,} \end{cases} \tag{39}$$

where we have set $\Delta_{\rm de} \equiv \delta_{\rm de}/\delta_{\rm m}$. Obviously, if we use $c_{\rm eff}^2 = 0$, then Equation (37) reduces to Equation (30), while in the case of the usual ΛCDM model, we need to a priori set $\delta_{\rm de} \equiv 0$.

Furthermore, substituting Equations (36) and (38) in Equation (37), we arrive at

$$-(1+z)\frac{d\gamma}{dz}\ln(\Omega_{\rm m}) + \Omega_{\rm m}^{\gamma} + 3w_{\rm de}\Omega_{\rm de}\left(\gamma - \frac{1}{2}\right) + \frac{1}{2} = \frac{3}{2}\Omega_{\rm m}^{1-\gamma}\mu. \tag{40}$$

Regarding the growth index evolution, we use the following phenomenological parameterization (see also Polarski & Gannouji 2008; Ishak & Dossett 2009; Wu et al. 2009; Bueno Belloso et al. 2011; Basilakos 2012; Basilakos & Pouri 2012;

Table 3
Statistical Results for Homogeneous (Clustered) DE Parameterizations Used in the Analysis

Model	PADE I	Simplified PADE I	PADE II	CPL	ΛCDM
k	7	6	7	6	4
$\chi^2_{\rm min}$	576.4(576.5)	576.4(576.7)	576.9(577.1)	576.5(576.7)	582.6
AIC	590.4(590.5)	588.4(588.7)	590.9(591.1)	588.5(588.7)	590.6
BIC	621.6(621.7)	615.1(615.4)	622.1(622.3)	615.2(615.4)	608.4

Note. These results are based on the expansion+growth rate data. The concordance ΛCDM model is shown for comparison.

Di Porto et al. 2012):

$$\gamma(a) = \gamma_0 + \gamma_1[1 - a(z)]. \tag{41}$$

Now, utilizing Equation (40) at the present time $z = 0$ and with the aid of Equation (41), we obtain (see also Polarski & Gannouji 2008)

$$\gamma_1 = \frac{\Omega_{\rm m0}^{\gamma_0} + 3w_{\rm de0}\left(\gamma_0 - \frac{1}{2}\right)\Omega_{\rm de0} + \frac{1}{2} - \frac{3}{2}\Omega_{\rm m0}^{1-\gamma_0}\mu_0}{\ln\Omega_{\rm m0}}, \tag{42}$$

where $\mu_0 = \mu(z = 0)$ and $w_{\rm de0} = w_{\rm de}(z = 0)$. Clearly, in order to predict the growth index evolution in DE models, we need to estimate the value of γ_0. For the current parameterization, it is easy to show that at high redshifts $z \gg 1$, the asymptotic value of $\gamma(z)$ is written as $\gamma_\infty \simeq \gamma_0 + \gamma_1$, while the theoretical formula of γ_∞ is given by Steigerwald et al. (2014),

$$\gamma_\infty = \frac{3(M_0 + M_1) - 2(H_1 + N_1)}{2 + 2X_1 + 3M_0}, \tag{43}$$

where the following quantities have been defined:

$$M_0 = \mu|_{\omega=0}, \quad M_1 = \frac{d\mu}{d\omega}\bigg|_{\omega=0} \tag{44}$$

and

$$N_1 = 0, \quad H_1 = -\frac{X_1}{2} = \frac{3}{2}w_{\rm de}(a)|_{\omega=0}, \tag{45}$$

where $\omega = \ln\Omega_{\rm m}(a)$. Obviously, for $z \gg 1$ we get $\Omega_{\rm m}(a) \to 1$ [or $\Omega_{\rm de}(a) \to 0$], which implies $\omega \to 0$. For more details regarding the theoretical treatment of (43), we refer the reader to Steigerwald et al. (2014). It is interesting to mention that the asymptotic value of the equation of state parameter for the current PADE cosmologies is written as

$$w_\infty \equiv w_{\rm de}(a \to 0) = \begin{cases} \frac{w_0 + w_1}{1 + w_2}, & \text{for PADE I} \\ \frac{w_0}{1 + w_1}, & \text{for Sim. PADE I} \\ \frac{w_1}{w_2}, & \text{for PADE II.} \end{cases} \tag{46}$$

At this point we are ready to present our growth index results:

1. *Homogeneous PADE parameterizations.* Here we set $\mu(a) = 1$ ($\Delta_{\rm de} \equiv 0$). From Equations (44) and (45), we find

$$\{M_0, M_1, H_1, X_1\} = \left\{1, 0, \frac{3w_\infty}{2}, -3w_\infty\right\},$$

and thus Equation (43) becomes

$$\gamma_\infty = \frac{3(w_\infty - 1)}{6w_\infty - 5}. \tag{47}$$

Lastly, inserting $\gamma_0 \simeq \gamma_\infty - \gamma_1$ into Equation (42) and utilizing Equations (46) and (47) together with the cosmological constraints of Table 4, we obtain

$$(\gamma_0, \gamma_1, \gamma_\infty) = \begin{cases} (0.555, -0.031, 0.524), & \text{for PADE I} \\ (0.558, -0.021, 0.537), & \text{for Sim. PADE} \\ (0.559, -0.017, 0.542), & \text{for PADE II.} \end{cases} \tag{48}$$

For comparison, we provide the results for the ΛCDM model and CPL parameterization, respectively. Specifically, we find $(\gamma_0, \gamma_1, \gamma_\infty)_\Lambda \simeq (0.556, -0.011, 0.545)$ and $(\gamma_0, \gamma_1, \gamma_\infty)_{\rm CPL} \simeq (0.561, -0.020, 0.541)$.

2. *Clustered PADE parameterizations.* Here the functional form of $\mu(a)$ is given by the second branch of Equation (39), which means that we need to define $\Delta_{\rm de}$. From Equation (33), we simply have $\Delta_{\rm de} = \frac{1 + w_{\rm de}}{1 - 3w_{\rm de}}$, and thus $\mu(a)$ takes the following form:

$$\mu(a) = 1 + (1 + 3c_{\rm eff}^2)\frac{\Omega_{\rm de}}{\Omega_{\rm m}}\frac{(1 + w_{\rm de})}{(1 - 3w_{\rm de})}. \tag{49}$$

In this case, from Equations (44) and (45) we obtain (for more details see the Appendix)

$$\{M_0, M_1, H_1, X_1\} = \left\{1, -\frac{(1 + w_\infty)(1 + 3c_{\rm eff}^2)}{1 - 3w_\infty}, \frac{3w_\infty}{2}, -3w_\infty\right\},$$

and from Equation (43) we find

$$\gamma_\infty \simeq \frac{3[(1 - 3w_\infty)(1 - w_\infty) - (1 + w_\infty)(1 + c_{\rm eff}^2)]}{(6w_\infty - 5)(3w_\infty - 1)}.$$

Notice that in the case of fully clustered PADE parameterizations ($c_{\rm eff}^2 = 0$), the previous expression becomes

$$\gamma_\infty \simeq \frac{3w_\infty(3w_\infty - 5)}{(6w_\infty - 5)(3w_\infty - 1)}. \tag{50}$$

For Equations (46) and (47), utilizing Equations (46)–(50) and the cosmological parameters of Table 4, we now find

$$(\gamma_0, \gamma_1, \gamma_\infty) = \begin{cases} (0.547, 0.005, 0.552), & \text{for PADE I} \\ (0.542, 0.012, 0.554), & \text{for Sim. PADE I} \\ (0.549, 0.003, 0.552), & \text{for PADE II.} \end{cases} \tag{51}$$

Table 4
Summary of the Best-fit Parameters for Homogeneous (Clustered) DE Parameterizations Using the Background + Growth Rate Data

Model	PADE I	Simplified PADE I	PADE II	CPL	ΛCDM
$\Omega_{\rm m}^{(0)}$	0.288 ± 0.010 (0.288 ± 0.010)	0.288 ± 0.010 (0.2888 ± 0.0099)	0.2721 ± 0.0097 (0.2723 ± 0.0098)	0.2875 ± 0.0095 (0.2882 ± 0.0093)	0.2902 ± 0.0090
h	0.681 ± 0.012 (0.681 ± 0.012)	0.680 ± 0.012 (0.679 ± 0.012)	0.684 ± 0.012 (0.683 ± 0.012)	0.681 ± 0.011 (0.680 ± 0.011)	0.6833 ± 0.0084
w_0	-0.856 ± 0.088 ($-0.874^{+0.086}_{-0.097}$)	-0.839 ± 0.038 (-0.836 ± 0.037)	-0.893 ± 0.075 (-0.896 ± 0.078)	$-0.81^{+0.10}_{-0.12}$ (-0.81 ± 0.10)	...
w_1	$0.07^{+0.37}_{-0.29}$ ($0.14^{+0.38}_{-0.29}$)	...	$0.41^{+0.26}_{-0.22}$ ($0.43^{+0.27}_{-0.22}$)	$-0.41^{+0.46}_{-0.37}$ ($-0.39^{+0.42}_{-0.36}$)	...
w_2	$-0.694^{+0.040}_{-0.036}$ ($-0.699^{+0.042}_{-0.038}$)	-0.388 ± 0.034 (-0.388 ± 0.035)	$-0.357^{+0.039}_{-0.033}$ ($-0.358^{+0.038}_{-0.034}$)	...	...
σ_8	0.751 ± 0.015 (0.755 ± 0.016)	0.751 ± 0.015 (0.758 ± 0.015)	0.771 ± 0.015 (0.771 ± 0.016)	0.751 ± 0.015 (0.756 ± 0.015)	0.744 ± 0.014
$w_{\rm de}(z=0)$	$-0.856(-0.874)$	$-0.839(-0.836)$	$-0.893(-0.896)$	$-0.81(-0.81)$	-1.0
$\Omega_{\rm de}(z=0)$	0.712(0.712)	0.712(0.7112)	0.7279(0.7277)	0.7125(0.7118)	0.7098

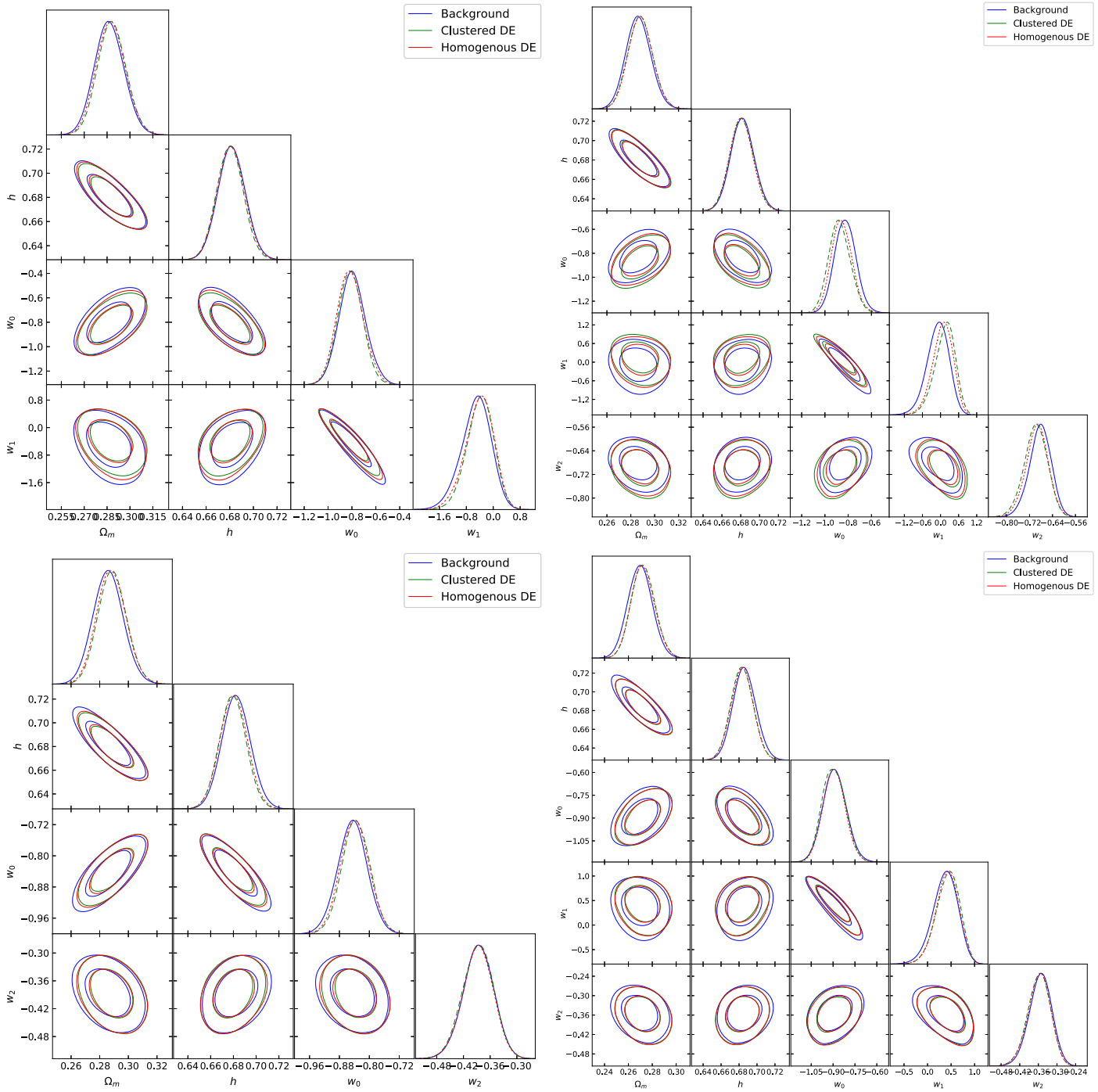

Figure 4. 1σ and 2σ likelihood contours for various planes using the solely expansion data (blue), and combined expansion and growth rate data for clustered (green) and homogeneous (red) DE parameterizations. The upper left (upper right) shows the results for CPL (PADE I) parameterization. The lower left (lower right) shows the results for simplified PADE I (PADE II) parameterization.

To this end, if the CPL parameterization is allowed to cluster, then the asymptotic value of the growth index is given by Equation (50), where $w_\infty = w_0 + w_1$. In this case, we find $(\gamma_0, \gamma_1, \gamma_\infty)_{\rm CPL} \simeq (0.539, 0.013, 0.552)$.

In Table 5, we provide a compact presentation of our numerical results, including the relative fractional difference $\Delta\gamma(\%) = [(\gamma - \gamma_\Lambda)/\gamma_\Lambda] \times 100$ between all DE parameterizations and the concordance Λ cosmology, in three distinct redshift bins. Overall, we find that the fractional deviation lies in the interval $\sim[-2.2\%, 0.3\%]$. We believe that relative differences of $|\Delta\gamma| \leqslant 1\%$ will be difficult to detect, even with the next generation of surveys, based mainly on Euclid (see Taddei & Amendola 2015). Using the latter forecast and the results presented in Section 4, we can now divide the current DE parameterizations into those that can be distinguished observationally and those that are practically indistinguishable from the ΛCDM model. The former DE parameterizations are as follows: homogeneous PADE I, clustered simplified PADE I, and clustered CPL. However, the reader has to remember that these results are based on utilizing cosmological parameters that have

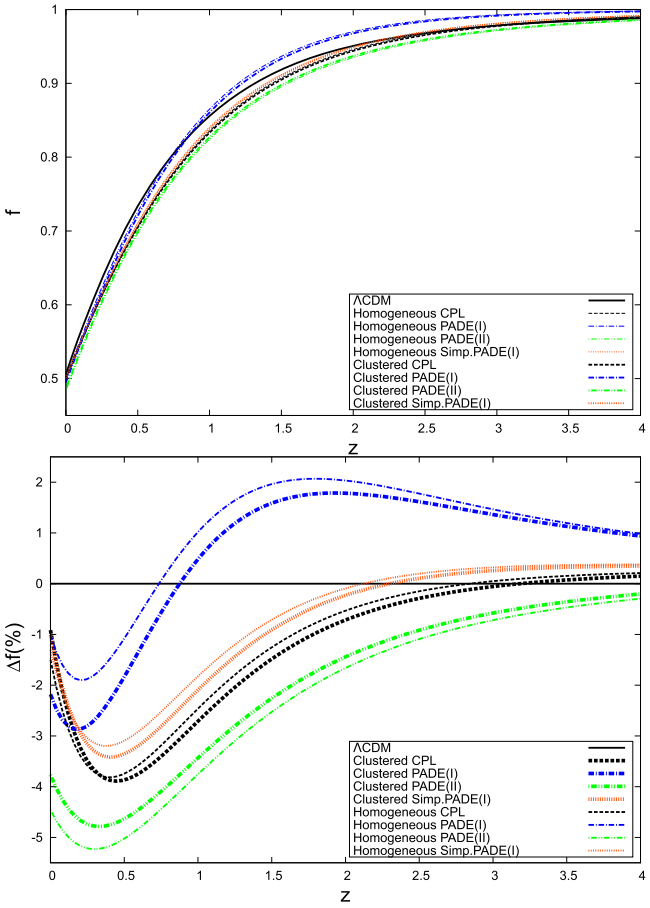

Figure 5. Redshift evolution of the growth rate function $f(z)$ (top panel) and the corresponding fractional difference $\Delta f(\%) = 100 \times [f(z) - f_\Lambda(z)]/f_\Lambda(z)$ (bottom panel). The different DE parameterizations are characterized by the colors and line types presented in the inner panels of the figure.

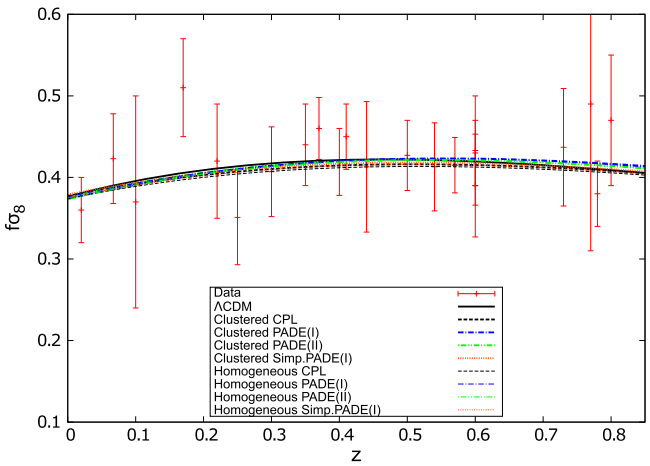

Figure 6. Comparison of the observed and theoretical evolution of the growth rate $f(z)\sigma_8(z)$ as a function of redshift z. Open squares correspond to the data. Line types and colors are explained in the inner plot of the figure.

been fitted by the present-day observational data (see Table 4). Therefore, if future observational data would provide slightly different values for the parameters of DE parameterizations, then the growth rate predictions of the studied DE parameterizations could be somewhat different than those derived here.

5. Conclusions

We studied the cosmological properties of various DE parameterizations in which the EoS parameter is given with the aid of the PADE approximation. Specifically, using different types of PADE parameterization, we investigated the behavior of various DE scenarios in the background and at the perturbation levels.

The main results of the present study are summarized as follows:

(i) Initially, using the latest expansion data, we performed a likelihood analysis in the context of the MCMC method. It is interesting to mention that the statistical performance of the MCMC method has been discussed in Capozziello et al. (2011) and references therein. Specifically, these authors showed that if we have a multidimensional space of the cosmological parameters, then the MCMC algorithm provides better constraints than other popular fitting procedures. The results of our analysis for the explored PADE cosmologies, including those of CPL and ΛCDM, can be found in Tables 1 and 2. Based on this analysis, we placed constraints on the model parameters and found that all DE parameterizations are consistent with the expansion data. In this framework, using the best-fit values, we found that only the PADE (II) parameterization remains in the quintessence regime ($1 < w_{\rm de} < 1/3$). The rest of the PADE parameterizations evolve in the phantom region ($w_{\rm de} < -1$) at high redshifts, while they enter in the quintessence regime at relatively low redshifts. Concerning the cosmic expansion, we found that prior to the present time, the Hubble parameter of the DE parameterizations (PADE and CPL) is ∼2%–3.5% larger than the ΛCDM cosmological model. We also showed that the transition redshift from decelerating to accelerating expansion in the context of PADE parameterizations is consistent with that (Farooq et al. 2017) using the cosmic chronometer $H(z)$ data. Note that similar results are found in the framework of the modified theory of gravities (Capozziello et al. 2014, 2015).

(ii) Next, we studied for the first time the growth of perturbations in homogeneous and clustered PADE cosmologies. First we used a joint statistical analysis involving the expansion data and the growth data in order to place constraints on σ_8. Second, based on the best-fit cosmological parameters, we computed the evolution of the growth rate of clustering $f(z)$. For the current DE parameterizations, we found that the growth rate function is lower than ΛCDM model at low redshifts, while the differences among the parameterizations are negligible at high redshifts. Third, following the notations of Steigerwald et al. (2014), we derived the functional form of the growth index (γ) of linear matter perturbations. Assuming that DE is homogeneous, we found the well-known asymptotic value of the growth index (namely $\gamma_\infty = \frac{3(w_\infty - 1)}{6w_\infty - 5}$ [$w_\infty = w(z \to \infty)$]), while in the case of clustered DE parameterizations, we obtained $\gamma_\infty \simeq \frac{3w_\infty(3w_\infty - 5)}{(6w_\infty - 5)(3w_\infty - 1)}$.

(iii) Finally, utilizing the fractional deviation between all DE parameterizations and the concordance Λ cosmology, we found that $\Delta\gamma \sim [-2.2\%, 0.3\%]$. We concluded that relative differences of $|\Delta\gamma| \leqslant 1\%$ will be difficult to detect, even with the next generation of surveys, based on Euclid (see Taddei & Amendola 2015). Combining the latter forecast and the results presented in Section 4, we divided the current DE parameterizations into those that can be distinguished observationally and those that are practically indistinguishable from ΛCDM. The

Table 5
Numerical Results

DE Status	DE Parameterization	γ_0	γ_1	Δ_{de0}	$\Delta\gamma(\%)$		
					$z < 0.5$	$0.5 \leqslant z < 1$	$1 \leqslant z < 1.5$
Homogeneous	PADE I	0.555	−0.031		−1.2	−1.8	−2.2
	Sim. PADE I	0.558	−0.021		−0.1	−0.4	−0.6
	PADE II	0.559	−0.017		0.15	−0.01	−0.15
	CPL	0.561	−0.02		0.3	−0.02	−0.2
Clustered	PADE I	0.547	0.005	0.035	−0.8	−0.5	−0.1
	Sim. PADE I	0.542	0.012	0.047	−1.4	−0.7	−0.2
	PADE II	0.549	0.003	0.028	−0.6	−0.4	−0.02
	CPL	0.539	0.013	0.055	−2	−1.5	−0.8

Note. The first and second columns indicate the status of DE and the corresponding parameterization. The third, fourth, and fifth columns show the γ_0, γ_1, and Δ_{de0} values. The remaining columns present the fractional relative difference between the DE parameterizations and the ΛCDM cosmology based on the cosmological parameters that appeared in Table 4.

former DE parameterizations are as follows: homogeneous PADE I, clustered simplified PADE I, and clustered CPL.

M.M. and A.M. acknowledge support from the Iran Science Elites Federation. D.F.M. acknowledges support from the Research Council of Norway, and the NOTUR facilities. S.B. acknowledges support by the Research Center for Astronomy of the Academy of Athens in the context of the program "Testing GR on Cosmological Scales" (ref. number 200/872).

Appendix
M_1 Coefficient for Clustered DE Models

Here we provide some details concerning the coefficient M_1 that appears in Equation (43). This coefficient is given in terms of the variable $\omega = \ln \Omega_m$ (see Section 4.1), which means that when $a \to 0$ ($z \gg 1$), we get $\Omega_m \to 1$ (or $\omega \to 0$). From Equation (44), we have

$$M_1 = \frac{d\mu}{d\omega}\bigg|_{\omega=0} = \Omega_m \frac{d\mu}{d\Omega_m}\bigg|_{\Omega_m=1}.$$

Of course, in the case of homogeneous DE (namely $\mu(a) = 1$), we simply find $M_1 = 0$. However, if DE is allowed to cluster, then the situation becomes quite different.

Indeed, using Equation (49), we obtain after some calculations

$$\frac{d\mu}{d\Omega_m} = (1 + 3c_{eff}^2)\frac{d}{d\Omega_m}\left(\frac{\Omega_{de}}{\Omega_m}\right)\frac{1 + w_{de}}{1 - 3w_{de}} + (1 + 3c_{eff}^2) \times \frac{\Omega_{de}}{\Omega_m}\frac{d}{d\Omega_m}\left(\frac{1 + w_{de}}{1 - 3w_{de}}\right),$$

where $\Omega_{de} = 1 - \Omega_m$,

$$\frac{d}{d\Omega_m}\left(\frac{\Omega_{de}}{\Omega_m}\right) = -\frac{1}{\Omega_m^2},$$

$$\frac{d}{d\Omega_m}\left(\frac{1 + w_{de}}{1 - 3w_{de}}\right) = \frac{d}{da}\left(\frac{1 + w_{de}}{1 - 3w_{de}}\right)\frac{da}{d\Omega_m},$$

with

$$\frac{d\Omega_m}{da} = \frac{3}{a}\Omega_m(1 - \Omega_m)w_{de} = \frac{3}{a}\Omega_m\Omega_{de}w_{de}.$$

Obviously, based on these equations, we arrive at

$$\Omega_m\frac{d\mu}{d\Omega_m} = -(1 + 3c_{eff}^2)\frac{1 + w_{de}}{\Omega_m(1 - 3w_{de})} + (1 + 3c_{eff}^2)\frac{a}{3\Omega_m w_{de}} \times \frac{d}{da}\left(\frac{1 + w_{de}}{1 - 3w_{de}}\right).$$

Taking the limit $\Omega_m \to 1$ ($a \to 0$) of the latter expression, we calculate M_1 as

$$M_1 = \Omega_m\frac{d\mu}{d\Omega_m}\bigg|_{\Omega_m=1} = -(1 + 3c_{eff}^2)\frac{1 + w_{de}}{1 - 3w_{de}}.$$

References

Abramo, L. R., Batista, R. C., Liberato, L., & Rosenfeld, R. 2007, JCAP, 11, 12
Abramo, L. R., Batista, R. C., Liberato, L., & Rosenfeld, R. 2008, PhRvD, 77, 067301
Abramo, L. R., Batista, R. C., Liberato, L., & Rosenfeld, R. 2009, PhRvD, 79, 023516
Adachi, M., & Kasai, M. 2012, PThPh, 127, 145
Akaike, H. 1974, ITAC, 19, 716
Akhoury, R., Garfinkle, D., & Saotome, R. 2011, JHEP, 04, 096
Alcaniz, J. S. 2004, PhRvD, 69, 083521
Allen, S. W., Schmidt, R. W., Ebeling, H., Fabian, A. C., & van Speybroeck, L. 2004, MNRAS, 353, 457
Amendola, L., Appleby, S., Bacon, D., et al. 2013, LRR, 16, 6
Anderson, L., Aubourg, E., Bailey, S., et al. 2013, MNRAS, 427, 3435
Anderson, L., Aubourg, E., Bailey, S., et al. 2014, MNRAS, 441, 24
Amendola, L., Kunz, M., & Sapone, D. 2008, JCAP, 0804, 013
Armendariz-Picon, C., Damour, T., & Mukhanov, V. F. 1999, PhLB, 458, 209
Armendariz-Picon, C., Mukhanov, V., & Steinhardt, P. J. 2001, PhRvD, 63, 103510
Armendariz-Picon, C., Mukhanov, V. F., & Steinhardt, P. J. 2000, PhRvL, 85, 4438
Aviles, A., Bravetti, A., Capozziello, S., & Luongo, O. 2014, PhRvD, 90, 043531
Baker, A., & Graves-Morris, P. 1996, Pade Approximants (Cambridge: Cambridge Univ. Press)
Ballesteros, G., & Riotto, A. 2008, Phys. Lett. B, 668, 171
Barboza, E. M., Alcaniz, J. S., Zhu, Z. H., & Silva, R. 2009, PhRvD, 80, 043521
Basilakos, S. 2012, IJMPD, 21, 50064
Basilakos, S. 2015, MNRAS, 449, 2151
Basilakos, S. 2016, PhRvD, 93, 083007
Basilakos, S., Bueno Sanchez, J., & Perivolaropoulos, L. 2009a, PhRvD, 80, 043530
Basilakos, S., Plionis, M., & Lima, J. A. S. 2010, PhRvD, 82, 083517
Basilakos, S., Plionis, M., & Sola, J. 2009b, PhRvD, 80, 083511

Basilakos, S., & Pouri, A. 2012, MNRAS, 423, 3761
Basilakos, S., & Sola, J. 2015, PhRvD, 92, 123501
Basilakos, S., & Stavrinos, P. 2013, PhRvD, 87, 043506
Basilakos, S., & Voglis, N. 2007, MNRAS, 374, 269
Basse, T., Bjaelde, O. E., Hamann, J., Hannestad, S., & Wong, Y. Y. 2014, JCAP, 1405, 021
Bassett, B. A., Brownstone, M., Cardoso, A., et al. 2008, JCAP, 0807, 007
Batista, R., & Pace, F. 2013, JCAP, 1306, 044
Batista, R. C. 2014, PhRvD, 89, 123508
Bean, R., & Doré, O. 2004, PhRvD, 69, 083503
Benjamin, J., Heymans, C., Semboloni, E., et al. 2007, MNRAS, 381, 702
Beutler, F., Blake, C., Colless, M., et al. 2011, MNRAS, 416, 3017
Blake, C., Brough, S., Colless, M., et al. 2011b, MNRAS, 415, 2876
Blake, C., Brough, S., Colless, M., et al. 2012, MNRAS, 425, 405
Blake, C., Kazin, E., Beutler, F., et al. 2011a, MNRAS, 418, 1707
Bonilla Rivera, A., & Farieta, J. G. 2016, arXiv:1605.01984
Bueno Belloso, A., García-Bellido, J., & Sapone, D. 2011, JCAP, 10, 10
Burles, S., Nollett, K. M., & Turner, M. S. 2001, ApJL, 552, L1
Caldwell, R. R. 2002, Phys. Lett. B, 545, 23
Caldwell, R. R., Dave, R., & Steinhardt, P. J. 1998, PhRvL, 80, 1582
Capozziello, S., Farooq, O., Luongo, O., & Ratra, B. 2014, PhRvD, 90, 044016
Capozziello, S., Lazkoz, R., & Salzano, V. 2011, PhRvD, 84, 124061
Capozziello, S., Luongo, O., & Saridakis, E. N. 2015, PhRvD, 91, 124037
Carroll, S. M. 2001, LRR, 380, 1
Chevallier, M., & Polarski, D. 2001, IJMP D, 10, 213
Chuang, C.-H., Prada, F., Cuesta, A. J., et al. 2013, MNRAS, 433, 3559
Cole, S., Percival, W. J., Peacock, J. A., et al. 2005, MNRAS, 362, 505
Contreras, C., Blake, C., Poole, G. B., et al. 2013, arXiv:1302.5178
Cooray, A., Huterer, D., & Baumann, D. 2004, PhRvD, 69, 027301
Copeland, E. J., Sami, M., & Tsujikawa, S. 2006, IJMP, D15, 1753
Corasaniti, P.-S., Giannantonio, T., & Melchiorri, A. 2005, PhRvD, 71, 123521
de Putter, R., Huterer, D., & Linder, E. V. 2010, PhRvD, 81, 103513
Dent, J. B., Dutta, S., & Weiler, T. J. 2009, PhRvD, 79, 023502
Di Porto, C., Amendola, L., & Branchini, E. 2012, MNRAS, 419, 985
Dossett, J., & Ishak, M. 2013, PhRvD, 88, 103008
Efstathiou, G. 1999, MNRAS, 310, 842
Eisenstein, D. J., Zehavi, I., Hogg, D. W., et al. 2005, ApJ, 633, 560
Elizalde, E., Nojiri, S., & Odintsov, S. D. 2004, PhRvD, 70, 043539
Erickson, J. K., Caldwell, R., Steinhardt, P. J., Armendariz-Picon, C., & Mukhanov, V. F. 2002, PhRvL, 88, 121301
Farooq, O., Madiyar, F. R., Crandall, S., & Ratra, B. 2017, ApJ, 835, 26
Fay, S. 2016, MNRAS, 460, 1863
Feng, C.-J., Shen, X.-Y., Li, P., & Li, X.-Z. 2012, JCAP, 1209, 023
Frampton, P. H., & Ludwick, K. J. 2011, EPJC, 71, 1735
Frieman, J., Turner, M., & Huterer, D. 2008, ARA&A, 46, 385
Fu, L., Semboloni, E., Hoekstra, H., et al. 2008, A&A, 479, 9
Fu, X.-X., Wu, P.-X., & Yu, H.-W. 2009, PhLB, 677, 12
Gannouji, R., Moraes, B., Mota, D. F., et al. 2010, PhRvD, 82, 124006
Gannouji, R., Moraes, B., & Polarski, D. 2009, JCAP, 0902, 034
Garriga, J., & Mukhanov, V. F. 1999, PhLB, 458, 219
Gaztanaga, E., Cabre, A., & Hui, L. 2009, MNRAS, 399, 1663
Gong, Y. 2008, PhRvD, 78, 123010
Gruber, C., & Luongo, O. 2014, PhRvD, 89, 103506
Hinshaw, G., Larson, D., Komatsu, E., et al. 2013, ApJS, 208, 19
Hu, W., & Scranton, R. 2004, PhRvD, 70, 123002
Ishak, M., & Dossett, J. 2009, PhRvD, 80, 043004
Jarosik, N., Bennett, C. L., Dunkley, J., et al. 2011, ApJS, 192, 14
Jassal, H. K., Bagla, J. S., & Padmanabhan, T. 2005, MNRAS, 356, L11
Koivisto, T., & Mota, D. F. 2007, PhLB, 644, 104
Komatsu, E., Dunkley, J., Nolta, M. R., et al. 2009, ApJS, 180, 330
Komatsu, E., Smith, K. M., Dunkley, J., et al. 2011, ApJS, 192, 18
Kowalski, M., Rubin, D., Aldering, G., et al. 2008, ApJ, 686, 749
Li, J., Yang, R., & Chen, B. 2014, JCAP, 1412, 043
Linder, E. V. 2003, PhRvL, 90, 091301
Linder, E. V., & Cahn, R. N. 2007, APh, 28, 481
Linder, E. V., & Jenkins, A. 2003, MNRAS, 346, 573
Llinares, C., & Mota, D. 2013, PhRvL, 110, 161101
Llinares, C., Mota, D. F., & Winther, H. A. 2014, A&A, 562, A78
Lue, A., Scoccimarro, R., & Starkman, G. D. 2004, PhRvD, 69, 124015
Malekjani, M., Basilakos, S., Davari, Z., Mehrabi, A., & Rezaei, M. 2017, MNRAS, 464, 1192
Malekjani, M., Naderi, T., & Pace, F. 2015, MNRAS, 453, 4148
Maor, I., Brustein, R., & Steinhardt, P. J. 2001, PhRvL, 86, 6
Mehrabi, A., Basilakos, S., Malekjani, M., & Davari, Z. 2015a, PhRvD, 92, 123513
Mehrabi, A., Basilakos, S., & Pace, F. 2015b, MNRAS, 452, 2930
Mehrabi, A., Malekjani, M., & Pace, F. 2015c, Ap&SS, 356, 129
Mehrabi, A., Pace, F., Malekjani, M., & Del Popolo, A. 2017, MNRAS, 465, 2687
Moresco, M., Cimatti, A., Jimenez, R., et al. 2012, JCAP, 1208, 006
Mota, D. F., Kristiansen, J. R., Koivisto, T., & Groeneboom, N. E. 2007, MNRAS, 382, 793
Mota, D. F., Sandstad, M., & Zlosnik, T. 2010, JHEP, 12, 051
Mota, D. F., Shaw, D. J., & Silk, J. 2008, ApJ, 675, 29
Naderi, T., Malekjani, M., & Pace, F. 2015, MNRAS, 447, 1873
Nazari-Pooya, N., Malekjani, M., Pace, F., & Jassur, D. M.-Z. 2016, MNRAS, 458, 3795
Nesseris, S., Blake, C., Davis, T., & Parkinson, D. 2011, JCAP, 1107, 037
Nesseris, S., & Perivolaropoulos, L. 2008, PhRvD, 77, 023504
Nesseris, S., & Sapone, D. 2015, IJMPD, 24, 1550045
Pace, F., Batista, R. C., & Del Popolo, A. 2014a, MNRAS, 445, 648
Pace, F., Fedeli, C., Moscardini, L., & Bartelmann, M. 2012, MNRAS, 422, 1186
Pace, F., Moscardini, L., Crittenden, R., Bartelmann, M., & Pettorino, V. 2014b, MNRAS, 437, 547
Pace, F., Waizmann, J. C., & Bartelmann, M. 2010, MNRAS, 406, 1865
Pade, H. 1892, Ann. Sci. Ecole Norm. Sup., 9, 1
Padmanabhan, N., Xu, X., Eisenstein, D. J., et al. 2012, MNRAS, 427, 2132
Padmanabhan, T. 2002, PhRvD, 66, 021301
Padmanabhan, T. 2003, PhR, 380, 235
Peebles, P. J., & Ratra, B. 2003, RvMP, 75, 559
Peebles, P. J. E. 1993, Principles of Physical Cosmology (Princeton, NJ: Princeton Univ. Press)
Percival, W. J., Reid, B. A., Eisenstein, D. J., et al. 2010, MNRAS, 401, 2148
Perlmutter, S., Aldering, G., Goldhaber, G., et al. 1999, ApJ, 517, 565
Planck Collaboration XIV 2016, A&A, 594, A14
Polarski, D., & Gannouji, R. 2008, PhLB, 660, 439
Reid, B. A., Samushia, L., White, M., et al. 2012, MNRAS, 426, 2719
Riess, A. G., Filippenko, A. V., Challis, P., et al. 1998, AJ, 116, 1009
Riess, A. G., et al. 2004, ApJ, 607, 665
Sahni, V., & Starobinsky, A. A. 2000, IJMPD, 9, 373
Sapone, D., & Majerotto, E. 2012, PhRvD, 85, 123529
Schwarz, G. 1978, AnSta, 6, 461
Seljak, U., Makarov, A., McDonald, P., et al. 2005, PhRvD, 71, 103515
Serra, P., Cooray, A., Holz, D. E., et al. 2009, PhRvD, 80, 121302
Silveira, V., & Waga, I. 1994, PhRvD, 50, 4890
Steigerwald, H., Bel, J., & Marinoni, C. 2014, JCAP, 1405, 042
Suzuki, N., Rubin, D., Lidman, C., et al. 2012, ApJ, 746, 85
Taddei, L., & Amendola, L. 2015, JCAP, 1502, 001
Tegmark, M., Strauss, M., Blanton, M., et al. 2004, PhRvD, 69, 103501
Tsujikawa, S., Gannouji, R., Moraes, B., & Polarski, D. 2009, PhRvD, 80, 084044
Wang, L., & Steinhardt, P. J. 1998a, ApJ, 508, 483
Wang, L.-M., & Steinhardt, P. J. 1998b, ApJ, 508, 483
Wei, H. 2008, PhLB, 664, 1
Wei, H., Yan, X.-P., & Zhou, Y.-N. 2014, JCAP, 1401, 045
Weinberg, D. H., Mortonson, M. J., Eisenstein, D. J., et al. 2013, PhR, 530, 87
Weinberg, S. 1989, RvMP, 61, 1
Wetterich, C. 2004, PhLB, 594, 17
Wu, P., Yu, H. W., & Fu, X. 2009, JCAP, 0906, 019
Yang, W., Xu, L., Wang, Y., & Wu, Y. 2014, PhRvD, 89, 043511
Zaninetti, L. 2016, Galax, submitted, arXiv:1602.06418
Zhou, Y.-N., Liu, D.-Z., Zou, X.-B., & Wei, H. 2016, EPJC, 76, 281